Science of the Total Environment 476–477 (2014) 447–459

Contents lists available at ScienceDirect

Science of the Total Environment

journal homepage: www.elsevier.com/locate/scitotenv

Coupling geochemical, mineralogical and microbiological approaches to assess the health of contaminated soil around the Almalyk mining and smelter complex, Uzbekistan

Nosir Shukurov [a,1], Obidjon Kodirov [a,1], Mirko Peitzsch [a,2], Michael Kersten [a,*], Stanislav Pen-Mouratov [b], Yosef Steinberger [b]

[a] Geosciences Institute, Johannes Gutenberg University, Mainz 55099, Germany
[b] The Mina and Everard Goodman Faculty of Life Sciences, Bar-Ilan University, Ramat Gan 52900, Israel

HIGHLIGHTS

- Soil samples were collected along a transect downwind of an industrial and mining area.
- Smelter particles were found in the heavy mineral fraction with metal-bearing weathering rims.
- Dissolved and exchangeable metal concentrations decreased with distance.
- Significant correlations were found between metal contents and microbiological health parameters.

ARTICLE INFO

Article history:
Received 22 August 2013
Received in revised form 30 December 2013
Accepted 7 January 2014
Available online 31 January 2014

Keywords:
Metals
Soil pollution
Bioindicator
Nematodes
Smelter impact
Microbial biomass
Metabolic quotient

ABSTRACT

This study describes the impact of airborne pollution resulting from mining and smelting activities on the soils of the Almalyk mining and industrial area (NE Uzbekistan). Samples were collected along a transect downwind of the industrial area. Enriched contents of some metals were found in the upper soil layers near the metallurgical complex (Zn ≤ 3010 mg kg^{-1}, Pb ≤ 630 mg kg^{-1}, Cd ≤ 30 mg kg^{-1}) which suggests that these metals were derived from local stack emissions. The morphology and internal microstructure of metal-bearing spherical particles found in the heavy mineral fraction suggest that these particles were probably a result of inefficient flue gas cleaning technique of the smelter. The highest metal concentrations were found also in soil solutions and exchangeable solid fractions from the first three locations, and decreased with increasing distance from the pollution source along transect. Thermodynamic equilibrium calculations suggest that the mobile metal pool in the contaminated soil is mainly controlled by dissolution of metal carbonates formed as weathering product of the metalliferous particles. The health of the microbiological soil ecosystem was assessed by measurements of basal respiration, nematode abundance, biomass-related C and N content, and microbial metabolic quotient qCO_2. Significant correlations were found between the dissolved metal content and the microbiological health parameters, a negative one for C_{mic}/C_{org} ratio, and a positive one for qCO_2. A negative correlation was found between the amount of nematodes and the metal contents suggesting that the contaminated soil has significant impact on the functioning of the microbiological community. A better understanding of the spatial variations in the whole ecosystem functioning due to airborne impact could be very useful for establishing suitable land use and best management practices for the polluted areas.

1. Introduction

Soils around mining and smelting sites may act as an important sink for mobile metal(loid)s introduced to the environment via fly ash, dust and leachates from the mine quarries, dumps and tailings (Birkefeld et al., 2007; Martín et al., 2007; Cecchi et al., 2008; Ettler et al., 2012). Clearly, the bioavailability and ecotoxicity of metals depend on their speciation. Therefore, to understand the impact of contamination from fly ash and dust it is necessary to study not only the total concentrations

* Corresponding author at: Geosciences Institute, Johannes Gutenberg University, Mainz 55099, Germany. Tel.: +49 6131 3924366; fax: +49 6131 3923070.
E-mail address: kersten@uni-mainz.de (M. Kersten).
[1] Permanent address: Institute of Geology and Geophysics, Uzbek Academy of Sciences, Tashkent 100041, Uzbekistan.
[2] Present address: Institute of Clinical Chemistry and Laboratory Medicine, TU Dresden, 01307 Dresden, Germany.

0048-9697/$ – see front matter © 2014 Elsevier B.V. All rights reserved.
http://dx.doi.org/10.1016/j.scitotenv.2014.01.031

of metals, but also their partition/distribution coefficients (K_d factors) and bioavailability (EPA, 1999; Weber and Karczewska, 2004). The bioavailability of metals is geochemically assessed by ion exchange (Peijnenburg et al., 2007). Single or sequential extraction schemes have primarily been developed to establish the mobility and availability of metal(loid)s and other toxic elements in soils and sediments contaminated by mine tailings (Fanfani et al., 1997; Cohen et al., 1998; Li and Thornton, 2001; Van Herck and Vandecasteele, 2001; Dold, 2003; Cappuyns et al., 2007; Pueyo et al., 2008; Favas et al., 2011). The extraction methods were also useful in screening waste from combustion and smelting (Kersten and Förstner, 1995; Vanek et al., 2008), and for evaluating potential remediation measures for smelter-ash contaminated soil (Nowack et al., 2010). However, metal ecotoxicity is not necessarily a simple function of the extractable metal present, but is controlled also by various physicochemical and biological co-factors, such as the pH of the soil, the organic matter and clay mineral content, the redox status, or the activity of the living biomass (Anderson and Domsch, 1990; Brookes, 1995; Neher, 2001; Van Gestel, 2008; Smolders et al., 2009). The complexity of these co-factors, and their considerable spatial and temporal variability in the field, make it difficult to predict metal ecotoxicity, and hence render environmental risk assessment more difficult. For this reason, chemical analyses alone are inadequate for the appropriate assessment of the health of soil and organisms (hereafter "soil health"), and should be corroborated by biological methods involving indicator organisms (Nahmani and Rossi, 2003; Jänsch et al., 2005; Yang et al., 2006; Yan et al., 2012).

The detrimental effects of metal(loid)s and other soil contaminants on soil health have been widely reported (Hattori, 1992; Bardgett et al., 1994; Kandeler et al., 1996; Klumpp et al., 2003). Measurements of the biomass of soil organisms, together with an understanding of their population dynamics, have been found to be a useful indicator of environmental pollution of various soil ecosystems (Ingham et al., 1986a, 1986b; Yeates et al., 2003). It is well known that metal contamination reduces soil respiration (Hattori, 1992), microbial biomass (Klumpp et al., 2003), invertebrate density and the resulting impact on trophic interactions (Vig et al., 2003; Caussy et al., 2003; Santorufo et al., 2012). In natural ecosystems, nematode abundance and community structure analyses were proved to be sensitive indicators of stress caused by soil pollutants and ecological disturbance (Sochova et al., 2006; Shao et al., 2008; Kapusta et al., 2011). The populations of omnivorous and predatory nematodes with a K-strategist type of life history appear to be sufficiently sensitive to metal pollution (Bongers and Bongers, 1998; Bakonyi et al., 2003), and the populations of several nematode taxa are significantly affected by the concentration of Cu, Ni, and Zn (Korthals et al., 1996a).

The present study focuses on the Almalyk mining and smelting complex, a major source of air and soil pollution in Uzbekistan (Kodirov and Shukurov, 2009). In a previous study, significant metal contamination and its impact on nematode population have already been reported for soils collected in this area (Shukurov et al., 2005). To date, however, there have been no studies of metal bioavailability in the polluted soils. Here we report data of a more extended triad-like ecological risk assessment applying in parallel different analysis methods. In our triad procedure, we couple a geochemical approach, involving both metal geochemical equilibrium modeling and kinetic extraction data, with an evaluation of the soil microbiological ecosystem. The triad-like ecotoxicity assessment approach has not yet been widely reported in the literature. The aims of our study are to (i) use microspectroscopic analysis and geochemical equilibrium modeling to assess the mechanisms controlling the bioavailability of the metals in the soils along a transect downwind the industrial complex, (ii) evaluate the impact of the metals on soil health using microbiological indicators such as the soil free-living nematode abundance, basal respiration, the C and N content of the microbial biomass, as well as microbial health indices such as the metabolic quotient, and (iii) examine the analytical data for any correlations between the chemical and biological parameters of the soil, with the ultimate aim of assessing the extent of the soil pollution in the area of interest.

2. Materials and methods

2.1. Sampling sites

The study site is located 65 km from Tashkent, the capital city of Uzbekistan, in the Akhangaran river valley between the Chatkal and Qurama mountain ranges (Western Himalayan Tien-Shan orogen). The industrial area lies in the floodplains of the Akhangaran river near the city of Almalyk (40°50′N–69°34′E). The Qurama Mountain ridge is rich in nonferrous metal resources, and in this area metal mines were founded in the early 50's. The Almalyk mining and smelting complex (AMSC) is the largest nonferrous mining company in Uzbekistan, producing refined copper, gold, silver, lead, metallic zinc, and other products. It has a mining capacity of about 25 Mio. metric tons of ore per year, and an annual metal production of 130,000 t Cu, 40,000 t Zn, and 80,000 t Pb (Levine and Wallace, 2010). However, AMSC started with no efficient flue gas cleaning facility, and the complex has become a major source of air pollution in the region. It is reported to emit about 100,000 t per year of harmful substances (including sulfur dioxide, black carbons, nitrogen oxides, sulfuric acid, metal(oid)s, etc.), which represents approximately 13% of all airborne emissions of these pollutants from point sources in Uzbekistan (UNECE, 2001).

The study area lies in a mountain valley with large variations in both seasonal and daily air temperature due to a continental climate with hot and dry summers and short, cold winters. The prevailing winds are westerly and south-westerly along the river valley. The average annual rainfall is between 100 and 200 mm, which is less than the rate of evaporation (UNECE, 2001). The study area is surrounded by a chain of mountains, which limits air circulation and exchange, thereby increasing the airborne pollution impact on soils and vegetation. Since 1994, the State Committee for Geology and Mineral Resources is carrying out routinely environmental monitoring in the Almalyk industrial area. This has revealed severe contamination of surface and groundwater, soil and vegetation (UNECE, 2001). The vegetation in the study area is mainly composed of annual and perennial plants, most notably *Astragalus*, *Stipa*, *Medicago*, and *Artemisia* genera, which prosper in the alkaline lithosols (FAO, 2003) with high levels of $CaCO_3$.

2.2. Soil sampling

Soil samples were collected in June 2005, when rainy weather softened the soil, in duplicate from two topsoil layers: 0–10 and 10–20 cm, at 11 equidistant (2 km apart) sampling plots (in total 44 soil samples 200 g each). The plots were aligned on a 20 km E–W transect along the Akhangaran river valley downwind of the AMSC pollution source which starts at the copper refinery and smelting factory, and ends in a rural grassland area near the town of Pskent (Fig. 1). The transect passes the Almalyk mineral fertilizer factory, industrial landfills (phosphogypsum, metallurgical slags), and agricultural lands (Fig. 1). The land use and characteristics of each sampling plot are as follows: L_1 (0 km, 40°51′40″N/69°33′18″E) grassland at the border of the Cu processing factory, L_2 (2 km, 40°51′41″N/69°32′4″E) grassland nearby the Cu smelter slag wastes and chemical factory, L_3 (4 km, 40°51′45″N/69°30′41″E) grassland nearby the phosphogypsum landfills of chemical factory, L_4 (6 km, 40°51′47″N/69°29′21″E) grassland in rural area, L_5 (8 km, 40°51′43″N/69°28′10″E) grassland in agricultural area, L_6 (10 km, 40°51′42″N/69°26′39″E) grassland in agricultural area, L_7 (12 km, 40°51′52″N/69°25′23″E) grassland in agricultural area, L_8 (14 km, 40°51′58″N/69°24′0″E) grassland in agricultural area, L_9 (16 km, 40°52′2″N/69°22′37″E) grassland in agricultural area, L_{10} (18 km, 40°52′10″N/69°21′18″E) grassland in rural area, and L_{11} (20 km, 40°52′12″N/69°19′52″E) grassland in rural area. Two samples were collected at each plot from each of the two soil layers (44 samples

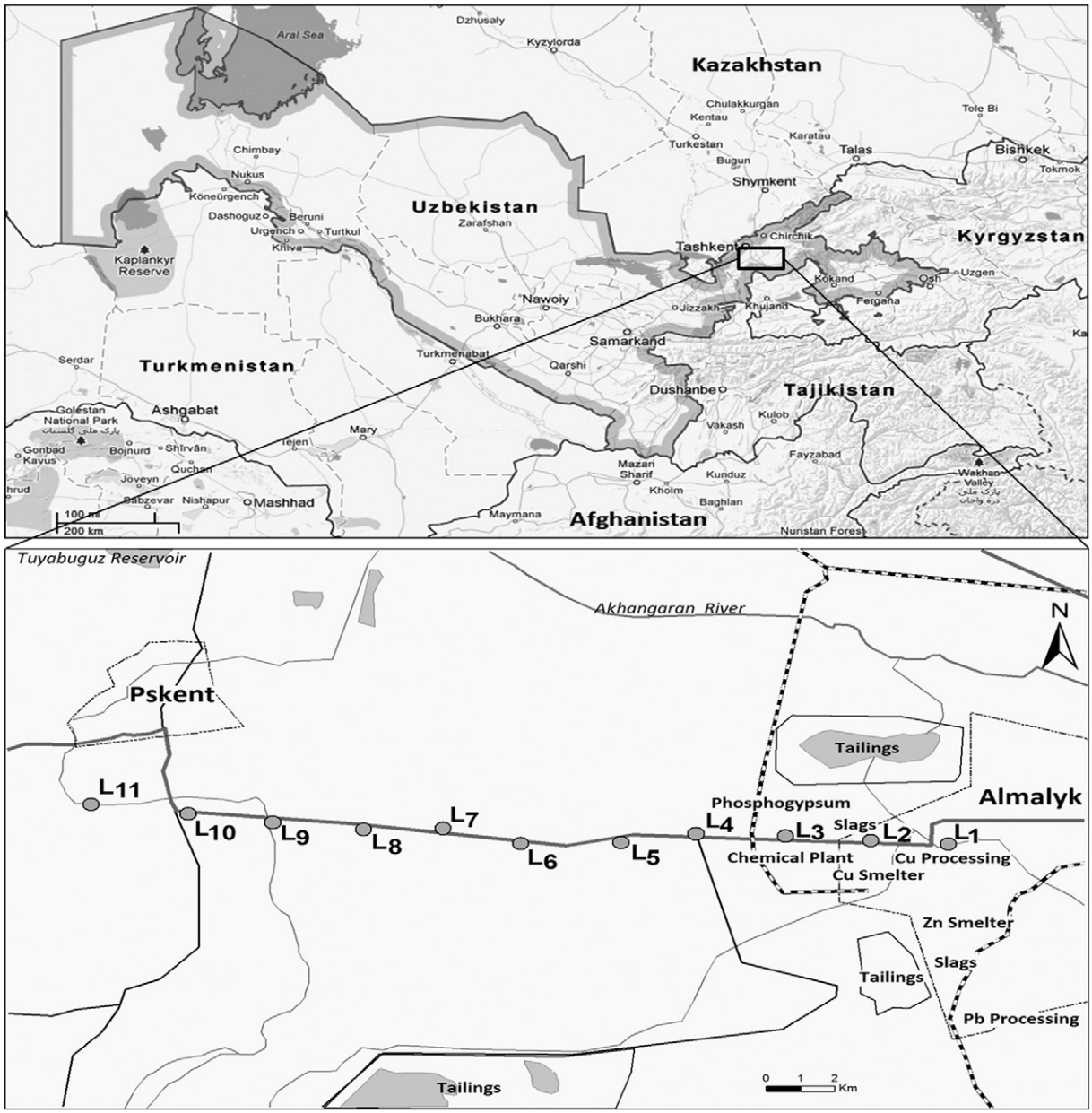

Fig. 1. Locations of the study sites along transect downwind of the Almalyk industrial area (L_1 — 0 km, L_2 — 2 km, L_3 — 4 km, L_4 — 6 km, L_5 — 8 km, L_6 — 10 km, L_7 — 12 km, L_8 — 14 km, L_9 — 16 km, L_{10} — 18 km, L_{11} — 20 km).

in total). The samples were transported in plastic bags to the laboratory, sieved (2 mm mesh) for plant detritus, and stored at 4 °C for two days prior to microbiological analysis.

2.3. Laboratory analysis

2.3.1. Soil physicochemical and metal analysis

The soils were air dried and passed through a 2-mm sieve prior to analysis. Residual soil moisture of the subsamples was measured gravimetrically as the percentage of dry mass by drying the samples to a constant weight at 105 °C. All chemical data presented in this study relies on dry weight basis. Soil pH was determined in H_2O (soil solution ratio 1:2) with a calibrated potentiometric glass electrode. Soil salinity was determined in soil extracts and expressed as specific conductivity (*SC* in mS cm^{-1}). Soluble cations (Ca^{2+}, K^+, Na^+) in these extracts were determined by flame photometer. Total organic carbon (C_{org}) was determined using a modified method of Rowell (1994). The method is based on the organic matter oxidation by K-dichromate. Total soluble nitrogen (*TSN*) was determined by adding 25 mL 0.01 M $CaCl_2$ to 10 g subsamples and shaking for 2 h (Houba et al., 1987). The amounts of *TSN* in the soil extracts were determined using an autoanalyzer device (Skalar Inc., The Netherlands).

Total element inventories (Cd, Cr, Cu, Ni, Pb, Pb, and Zn) for the soil samples were obtained in duplicate using wavelength dispersive X-ray fluorescence spectrometry (PANalytical MagiX Pro XRF with rhodium anode X-ray tube operated at 3.6 kV). The finely ground samples were cast to powder pellets under a pressure of 7 t with some epoxy resin admixture in a 30-mm die of a Herzog hydraulic press. Analytical quality assurance/quality control (QA/QC) was performed using certified reference materials (Montana soil CRM's 2710 and 2711). The common sequential extraction procedure described by Tessier et al. (1979) was used for fractionating of Cu, Pb, Zn, Cd, Ni, and Cr in soil. Five fractions (F1–F5) were thus produced according to the scheme with extracting agents as compiled in Table 1. The supernatant was decanted and centrifuged at 4000 rpm for 30 min, and then the residues were washed by deionized water and centrifuged for a further 30 min. All extracts

Table 1
Chemical reagents and analytical conditions for the sequential extraction procedure based on the original protocol by Tessier et al. (1979).

Steps and Fractions	Operational definition	Chemical reagents and conditions
F1	NaOAc-exchangeable	Sample of 1 g digested with 8 mL of 1 M NaOAc at pH 8.2 for one hour with continuous agitation at room temperature;
F2	HOAc-exchangeable and carbonates	Residue from step 1 leached with 8 mL of 1 M sodium acetate adjusted to pH 5.0 with acetic acid at room temperature for 5 h;
F3	Acid-reducible	Digesting the residue from step 2 with 20 mL of 0.04 M hydroxylammonium hydrochloride in 25% (v/v) acetic acid at 90 °C, with occasional agitation for 6 h;
F4	Oxidizable	Digesting the residue from step 3 twice with a mixture of 3 mL 0.02 M HNO_3 and 5 mL 30% hydrogen peroxide at 85 °C for 2 h, with occasional agitation until almost dryness, followed by a 30 min digestion of the cake by 50 mL of ammonium acetate (1 M adjusted to pH 2 with HNO_3) at room temperature;
F5	Residual	Microwave digestion by an aqua regia mixture of HNO_3 and HCl.

were stored in a fridge prior to the analysis of the metal concentrations using ICP-OES (Spectro Ciros Vision). Analytical quality assessment was performed on the basis of the certified reference materials NIST 2710/2711 (Montana Soil, USA). Differences between total concentrations measured by XRF and the recovery rates of the sequential extraction procedure (sum of the five steps F1–F5 for each metal) are compiled in Table 2.

Subsamples of both 0–10 and 10–20 cm layers from every second plot sampled along transect were pooled and homogenized to measure the dissolved metal concentrations. These subsamples were re-wetted up to a 50% water holding capacity (WHC = 47 ± 6%) in preparation for an incubation process mimicking a winter rain flush. Approximately 100 g of such a subsample was placed in a plastic beaker. Two micro-suction cups (0.3 mL) made of a 0.45 μm nylon membrane, with polyethylene substructure and cover shield (Ecotech, Germany), were inserted a few millimeter into the wet soil. The suction cup material was chosen to minimize adsorption artifacts (Rais et al., 2006). The beaker was covered by a watch glass to prevent evaporation during incubation. All incubation experiments were carried out in duplicate at room temperature (23 ± 2 °C). To extract soil solution by sampling followed by centrifugation is operationally strongly biased, and, because sampling is destructive, does not allow for time lapse studies with a limited amount of subsamples available. One pair of suction cups was removed and jet washed after incubation for 4, 9.5, 24, 72, and 120 h, respectively. The acidified micro-suction cup solutions were analyzed using ICP-MS (Agilent 7700, Germany). To provide a blank quality control, solutions were derived for analysis from suction cups deployed in pure Milli-Q water.

2.3.2. Mineralogical analysis

Particle size fractionation was carried out by sieving <63 μm. The fine-grained fraction was then subjected additionally to gravity separation of the heavy mineral fraction using 1,1,2,2-tetrabromoethane (TBE, 2.95 g cm^{-3} at 20 °C). X-ray diffraction analysis was used to determine phase associations in the fine-grained heavy mineral fractions using a Siemens XRD D-500 instrument. The *d*-spacings obtained were compared with the JCPDS (International Center for Powder Diffraction Data, Swarthmore, USA) inorganic compound database using the DIFRAC + software. The heavy mineral grains then were embedded in epoxy resin. The cured specimens were cut, polished and carbon-coated to produce the smooth surfaces essential to achieve high quality backscattered electron (BE) images and X-ray fluorescence maps using electron microprobe analysis. The Jeol JXA 8900 instrument was equipped with both energy-dispersive (EDX) and wavelength-dispersive (WDX) X-ray fluorescence detector channels. The BE imaging was used to locate metal-bearing particles by their brightness. The chemical identity and heterogeneity of the metal-bearing particles were then traced by X-ray mapping of selected elements. The EDX channels were used for rapid screening and major element mapping, and the WDX channel was used for the metals in cases where EDX could not separate peak overlaps, e.g., of S and Pb.

Table 2
Recovery rates of the sequential extraction procedure.

Sampling locations	Depth cm	Zn		Cu		Pb		Cd	
		XRF − Σ(F1–F5)[a] mg kg^{-1}	Recovery[b] %	XRF − Σ(F1–F5) mg kg^{-1}	Recovery %	XRF − Σ(F1–F5) mg kg^{-1}	Recovery %	XRF − Σ(F1–F5) mg kg^{-1}	Recovery %
L_1 − 0 km	0–10	309	89	57	95	30	95	1.7	94
	10–20	208	77	63	93	49	91	8.1	71
L_3 − 4 km	0–10	136	83	58	92	22	90	0.8	94
	10–20	219	75	47	94	10	93	2.3	64
L_5 − 8 km	0–10	10	94	17	88	26	71	0.4	84
	10–20	7.8	93	21	84	15	76	0.3	85
L_7 − 12 km	0–10	17	89	8.8	88	12	71	0.5	70
	10–20	4.5	96	5.2	90	16	76	0.6	74
L_9 − 16 km	0–10	6.4	93	3.7	91	24	63	0.7	71
	10–20	9.6	94	1.5	96	18	70	1.3	47
L_{11} − 20 km	0–10	4.0	95	8.0	83	23	64	0.6	75
	10–20	8.9	89	6.5	85	20	68	0.2	88
SRM 2710		555	93	499	83	340	94	1.3	94
SRM 2711		29	92	11	90	44	96	2.2	95

Data are means of four replicates.
[a] XRF − Σ(F1–F5) − difference between the total metal concentration measured by XRF and the sum of the five steps in the sequential metal extraction.
[b] Recovery rate − Σ(F1–F5) / XRF × 100.

2.3.3. Microbiological analysis

Soil microbial biomass carbon was determined using the classical chloroform fumigation incubation method (Heinemayer et al., 1989; Sparling and West, 1990; Kaiser et al., 1992). Soil sample pellets (10 g) were adjusted to 40% WHC, and fumigated in a $CHCl_3$-saturated atmosphere in a desiccator for 24 h. Fumigated and (for control) non-fumigated subsamples were then transferred to closed 0.5 L glass vessels and incubated for 10 days at 25 °C in the dark. Gas chromatography (GC-8A, Shimadzu) was used to measure the CO_2 concentration in the head space of the glass vessels. The microbial biomass carbon was calculated as C_{mic} = [(CO_2–C from fumigated soil) − (CO_2–C from control sample)] / k_C, and given in units of μg C g^{-1} soil. A k_C value of 0.41 was used as proposed by Anderson and Domsch (1990). The basal respiration R_B (μg g^{-1} d^{-1}) was calculated from the temporal evolution of the CO_2–C in the non-fumigated control sample. The metabolic quotient (qCO_2) was calculated as the ratio of R_B to C_{mic} and was given in units of (μg CO_2–C) (μg C_{mic})$^{-1}$ day^{-1} as described in Anderson and Domsch (1990). There is a direct correlation between C_{mic} and C_{org} values, and the dimensionless ratio C_{mic}/C_{org} known as the microbial coefficient was therefore additionally determined because it allows the determination of substrate bioavailability. The samples that were used to measure C_{mic} values were also used to measure soil microbial biomass nitrogen N_{mic} applying the classical method by Sparling and Zhu (1993). The N_{mic} values were calculated as the difference between the *TSN* values measured in the fumigated and non-fumigated (control) samples as $N_{mic} = \Delta TSN / k_{EN}$, using a k_{EN} value of 0.54 (Joergensen and Mueller, 1996).

Nematode population was measured by extracting the organisms from 100 g soil subsamples using the classical Baermann funnel procedure (Cairns, 1960). The thus recovered organisms were preserved in formaldehyde solution, and identified to genus level (where possible) using an inverted compound optical microscope (Steinberger and Sarig, 1993). For the nematode community structure analyses, the species are divided into groups according to their feeding habits. The organisms were thus categorized into the following trophic groups: (i) bacteriovores (*BF*), (ii) fungivores (*FF*), (iii) plant-parasites (*PP*), and (iv) omnivore-predators (*OP*; Steinberger and Loboda, 1991; Steinberger and Sarig, 1993; Liang et al., 2000).

Table 4
Univariate analysis of variance (ANOVA) for soil conditions along the 20 km transect downwind of AMSC emission source.

Index	Location		Depth	
	F-test	p-Value[a]	F-test	p-Value
Total organic carbon (C_{org})	4.4	0.0003	16.5	0.0002
Total soluble nitrogen (*TSN*)	3.0	0.006	2.9	NS[b]
Basal respiration (R_B)	2.1	0.05	6.6	0.01
Microbial biomass carbon (C_{mic})	4.9	0.0001	3.3	NS
Metabolic quotient (qCO_2)	2.4	0.02	0.2	NS
Microbial coefficient — C_{mic}/C_{org}	3.4	0.003	1.0	NS
Total nematode abundance (T_{Nem})	1.3	NS	0.8	NS
Ca^{2+}	3.5	0.002	0.1	NS
Na^+	1.5	NS	1.0	NS
K^+	3.2	0.004	5.4	0.03
Zn_{total}[c]	13.4	<0.0001	8.5	0.006
Cu_{total}	59.5	<0.0001	5.2	0.03
Pb_{total}	10.5	<0.0001	9.7	0.003
Cd_{total}	12.4	<0.0001	6.9	0.003
Cr_{total}	38.8	<0.0001	0.4	NS
Ni_{total}	17.2	<0.0001	0.1	NS

[a] p-Values calculated according to 44 samples sampled in duplicate from the 11 locations and two depths.
[b] NS — difference non-significant.
[c] Me_{total} — Total metal concentrations measured by XRF.

2.3.4. Statistical analysis

All data were subjected to a statistical analysis using the SAS model (ANOVA, Duncan's multiple range test and Pearson correlation coefficient) and were used to evaluate differences between separate means. The datasets were first log-transformed and then tested for normality by the Shapiro–Wilk test using the statistical software package Statistica 4.3. ANOVA followed by Tukey's HSD test to establish the significance of differences between sampling locations along transect. Linear regression between abiotic and biotic parameters for all soil samples was then tested for correlation applying Pearson correlation coefficients with significance levels of $p < 0.05^*$ and $p < 0.01^{**}$, and inserted in the text and tables but not in separate figures.

Table 3
Sampling locations and main physicochemical properties of soils from the 11 sampling plots in two soil depths along the 20 km transect in Almalyk mining and smelting area.

Sampling locations	Depth cm	pH	Ca^{+2}	Na^+	K^+	C_{org}[a]	TSN[b]
			mg L^{-1}	mg L^{-1}	mg L^{-1}	%	mg L^{-1}
L_1 — 0 km	0–10	7.9 ± 0.1	51 ± 3.5	0.3 ± 0.1	5.5 ± 0.7	0.5 ± 0.1	10.2 ± 2.3
	10–20	7.9 ± 0.2	51 ± 3.5	0.3 ± 0.1	3.0 ± 0.6	0.5 ± 0.1	2.3 ± 0.8
L_2 — 2 km	0–10	7.7 ± 0.2	61 ± 2.8	0.3 ± 0.1	10.0 ± 1.7	0.8 ± 0.1	7.1 ± 2.4
	10–20	7.7 ± 0.1	59 ± 2.5	0.3 ± 0.1	7.0 ± 0.9	0.7 ± 0.1	4.9 ± 0.5
L_3 — 4 km	0–10	7.8 ± 0.2	53 ± 8.0	0.3 ± 0.1	3.7 ± 1.3	0.6 ± 0.1	6.4 ± 1.4
	10–20	7.8 ± 0.1	48 ± 0.1	0.3 ± 0.1	2.3 ± 1.2	0.5 ± 0.1	3.8 ± 1.6
L_4 — 6 km	0–10	7.8 ± 0.1	48 ± 4.5	0.3 ± 0.1	17.0 ± 2.2	0.7 ± 0.1	8.6 ± 3.3
	10–20	8.1 ± 0.1	50 ± 2.9	0.4 ± 0.1	2.7 ± 0.6	0.6 ± 0.1	6.0 ± 1.2
L_5 — 8 km	0–10	7.9 ± 0.1	37 ± 3.5	0.3 ± 0.1	3.0 ± 0.6	0.5 ± 0.1	2.4 ± 0.2
	10–20	7.9 ± 0.2	42 ± 3.5	0.3 ± 0.1	4.5 ± 0.6	0.5 ± 0.1	2.7 ± 0.7
L_6 — 10 km	0–10	7.9 ± 0.1	57 ± 4.8	0.3 ± 0.1	20.0 ± 1.5	1.2 ± 0.2	12.3 ± 3.2
	10–20	8.1 ± 0.2	54 ± 2.5	0.4 ± 0.1	9.0 ± 0.7	1.1 ± 0.3	11.3 ± 2.9
L_7 — 12 km	0–10	7.9 ± 0.1	46 ± 2.8	0.3 ± 0.1	17.0 ± 1.4	0.9 ± 0.1	6.8 ± 1.7
	10–20	8.1 ± 0.1	42 ± 3.5	0.4 ± 0.1	16.0 ± 0.7	0.6 ± 0.1	3.9 ± 0.6
L_8 — 14 km	0–10	8.1 ± 0.1	51 ± 2.9	0.4 ± 0.1	4.8 ± 0.6	0.9 ± 0.2	6.7 ± 1.6
	10–20	8.0 ± 0.1	54 ± 4.8	0.3 ± 0.1	4.5 ± 0.3	0.7 ± 0.2	8.1 ± 2.6
L_9 — 16 km	0–10	8.1 ± 0.1	56 ± 3.5	0.4 ± 0.1	8.5 ± 0.7	0.6 ± 0.1	6.8 ± 1.6
	10–20	8.2 ± 0.1	51 ± 2.9	0.4 ± 0.1	5.0 ± 0.2	0.5 ± 0.1	5.8 ± 0.9
L_{10} — 18 km	0–10	8.2 ± 0.2	65 ± 2.3	0.4 ± 0.1	19.0 ± 0.5	0.8 ± 0.2	13.7 ± 3.5
	10–20	8.1 ± 0.3	66 ± 2.2	0.4 ± 0.1	16.0 ± 1.5	0.6 ± 0.1	11.2 ± 2.6
L_{11} — 20 km	0–10	8.2 ± 0.1	46 ± 2.8	0.4 ± 0.1	13.0 ± 0.6	0.8 ± 0.1	6.1 ± 0.7
	10–20	8.1 ± 0.1	46 ± 2.8	0.4 ± 0.1	11.0 ± 0.6	0.6 ± 0.1	5.1 ± 0.8

Data are means of two replicates, ±SD.
[a] Soil organic carbon.
[b] Total soluble nitrogen.

Table 5
Contaminant metal concentrations in soil samples along the 20 km transect downwind of the AMSC emission source.

Sampling locations	Soil depth cm	Zn			Cu			Pb			Cd		
		Total mg kg^{-1}	Exchangeable mg kg^{-1}	Dissolved μg L^{-1}	Total mg kg^{-1}	Exchangeable mg kg^{-1}	Dissolved μg L^{-1}	Total mg kg^{-1}	Exchangeable mg kg^{-1}	Dissolved μg L^{-1}	Total mg kg^{-1}	Exchangeable mg kg^{-1}	Dissolved μg L^{-1}
L_1 — 0 km	0–10	3012 ± 235	1.9 ± 0.1	2584 ± 258	1117 ± 79	5.7 ± 2.8	789 ± 85	628 ± 38	1.9 ± 0.1	4.5 ± 0.7	30.3 ± 2.0	0.8 ± 0.2	22 ± 1.9
	10–20	2901 ± 333	1.6 ± 0.1	–	951 ± 56	3.9 ± 2.1	–	549 ± 57	1.2 ± 0.3	–	26.8 ± 2.2	0.6 ± 0.1	–
L_2 — 2 km	0–10	912 ± 22	–	–	773 ± 47	–	–	143 ± 12	–	–	5.7 ± 0.6	–	–
	10–20	889 ± 38	–	–	698 ± 91	–	–	127 ± 12	–	–	5.7 ± 0.3	–	–
L_3 — 4 km	0–10	851 ± 40	0.5 ± 0.1	982 ± 550	781 ± 48	2.0 ± 0.3	101 ± 8	188 ± 53	0.9 ± 0.1	1.2 ± 0.5	9.6 ± 4.1	0.7 ± 0.2	27 ± 10
	10–20	816 ± 62	0.4 ± 0.1	–	629 ± 129	1.7 ± 0.4	–	162 ± 57	1.1 ± 0.2	–	9.6 ± 4.0	0.6 ± 0.1	–
L_4 — 6 km	0–10	198 ± 34	–	–	199 ± 37	–	–	100 ± 11	–	–	1.1 ± 0.6	–	–
	10–20	159 ± 22	–	–	155 ± 10	–	–	84 ± 3	–	–	1.2 ± 0.5	–	–
L_5 — 8 km	0–10	147 ± 32	0.3 ± 0.1	255 ± 185	133 ± 22	1.0 ± 0.1	55 ± 15	76 ± 7	0.6 ± 0.1	1.2 ± 0.3	0.8 ± 0.3	0.4 ± 0.1	1.7 ± 0.5
	10–20	116 ± 11	0.2 ± 0.1	–	125 ± 18	0.9 ± 0.1	–	68 ± 7	0.7 ± 0.1	–	0.5 ± 0.3	0.3 ± 0.1	–
L_6 — 10 km	0–10	227 ± 26	–	–	152 ± 9	–	–	105 ± 5	–	–	1.8 ± 0.8	–	–
	10–20	179 ± 27	–	–	118 ± 22	–	–	85 ± 12	–	–	2.0 ± 0.6	–	–
L_7 — 12 km	0–10	163 ± 24	0.2 ± 0.1	122 ± 43	80 ± 12	0.7 ± 0.2	36 ± 8	81 ± 9	1.5 ± 0.1	1.0 ± 0.3	2.3 ± 0.3	0.3 ± 0.0	5.2 ± 3.1
	10–20	101 ± 14	0.1 ± 0.0	–	58 ± 7	0.4 ± 0.1	–	75 ± 7	1.1 ± 0.7	–	1.7 ± 0.3	0.3 ± 0.0	–
L_8 — 14 km	0–10	141 ± 28	–	–	80 ± 11	–	–	91 ± 7	–	–	2.1 ± 0.3	–	–
	10–20	112 ± 37	–	–	63 ± 10	–	–	85 ± 6	–	–	2.1 ± 0.3	–	–
L_9 — 16 km	0–10	92 ± 1	0.1 0.0	143 ± 38	39 ± 0.7	0.2 ± 0.0	15 ± 2	62 ± 3	0.4 ± 0.1	1.3 ± 0.5	2.3 ± 0.3	0.3 ± 0.1	1.0 ± 0.6
	10–20	87 ± 1	0.1 ± 0.0	–	38 ± 0.7	0.2 ± 0.0	–	60 ± 2	0.3 ± 0.1	–	2.4 ± 0.1	0.2 ± 0.0	–
L_{10} — 18 km	0–10	109 ± 13	–	–	62 ± 10	–	–	67 ± 7	–	–	2.1 ± 0.6	–	–
	10–20	97 ± 10	–	–	48 ± 13	–	–	63 ± 6	–	–	2.3 ± 0.3	–	–
L_{11} — 20 km	0–10	85 ± 9	0.1 ± 0.0	19 ± 9	45 ± 6	0.4 ± 0.1	22 ± 3	64 ± 6	0.5 ± 0.1	1.1 ± 0.3	2.0 ± 0.3	0.4 ± 0.1	2.2 ± 1.2
	10–20	81 ± 6	0.1 ± 0.0	–	40 ± 3	0.3 ± 0.1	–	60 ± 3	0.3 ± 0.0	–	1.7 ± 0.3	0.4 ± 0.1	–

Data are means ± SD of duplicate sampling and analysis for the XRF-total and NaOAc-exchangeable (from step F1 of sequential extraction) concentrations, and means of duplicates at five different times ± SD for the dissolved metals concentration, as indicated in the methods section.

3. Results

3.1. Soil characteristics

The soils were weakly alkaline, with a pH ranging from 7.7 to 8.2 (Table 3). The *TSN* content varied considerably among sampling sites, with respective values ranging from 2.3 to 13.7 mg L^{-1} and significant differences between sampling locations ($p < 0.006$). The C_{org} concentrations were around 0.5–0.9%, with generally higher content in upper soil layer, but also a sharp increase at sampling location L_6, reaching a mean value of 1.2% in the topsoil layer (Tables 3 and 4). The cation status as given by the average value of the activity ratio $a_{K+}/\sqrt{a_{Ca}^{2+}} = 5.2 \cdot 10^{-3} \pm 2.4 \cdot 10^{-3}$ $mol^{1/2}$ $L^{-1/2}$ indicates a relatively weak nutritional status of the grassland soils, except at locations L_6, L_7, and L_{10}, where a higher average ratio of $15.7 \cdot 10^{-3} \pm 4.9 \cdot 10^{-3}$ $mol^{1/2}$ $L^{-1/2}$ indicates some fertilization activity. The water soluble Ca^{2+} concentrations are, however, also relatively low, except at location L_1 (Table 3). A spatial comparison of the cation content revealed no significant differences in the concentration of water soluble K^+ and Na^+ between both soil layers. However, the trend lines showed moderate rising of both cations in soil solution by distance from the smelter along transect (Table 3).

3.2. Metal concentrations and sequential extraction results

The amounts of Zn, Cu, Pb, and Cd found in the samples significantly ($p < 0.0001$) decreased with distance along transect (Tables 4 and 5). The highest enrichment of the metals Zn, Pb, and Cd was found in topsoil near the Almalyk metal smelter (location L_1), with mean values of 3012 mg kg^{-1}, 628 mg kg^{-1}, and 30 mg kg^{-1}, respectively. These metals are known to become easily volatilized in high temperature processes. The proximity of L_1 to the smelter suggests that local stack emissions are the likely source of this contamination. The concentrations of Zn, Cu, and Pb were lower at the 10–20 cm sampling depth, than at 0–10 cm (albeit not significantly, because variability for samples taken

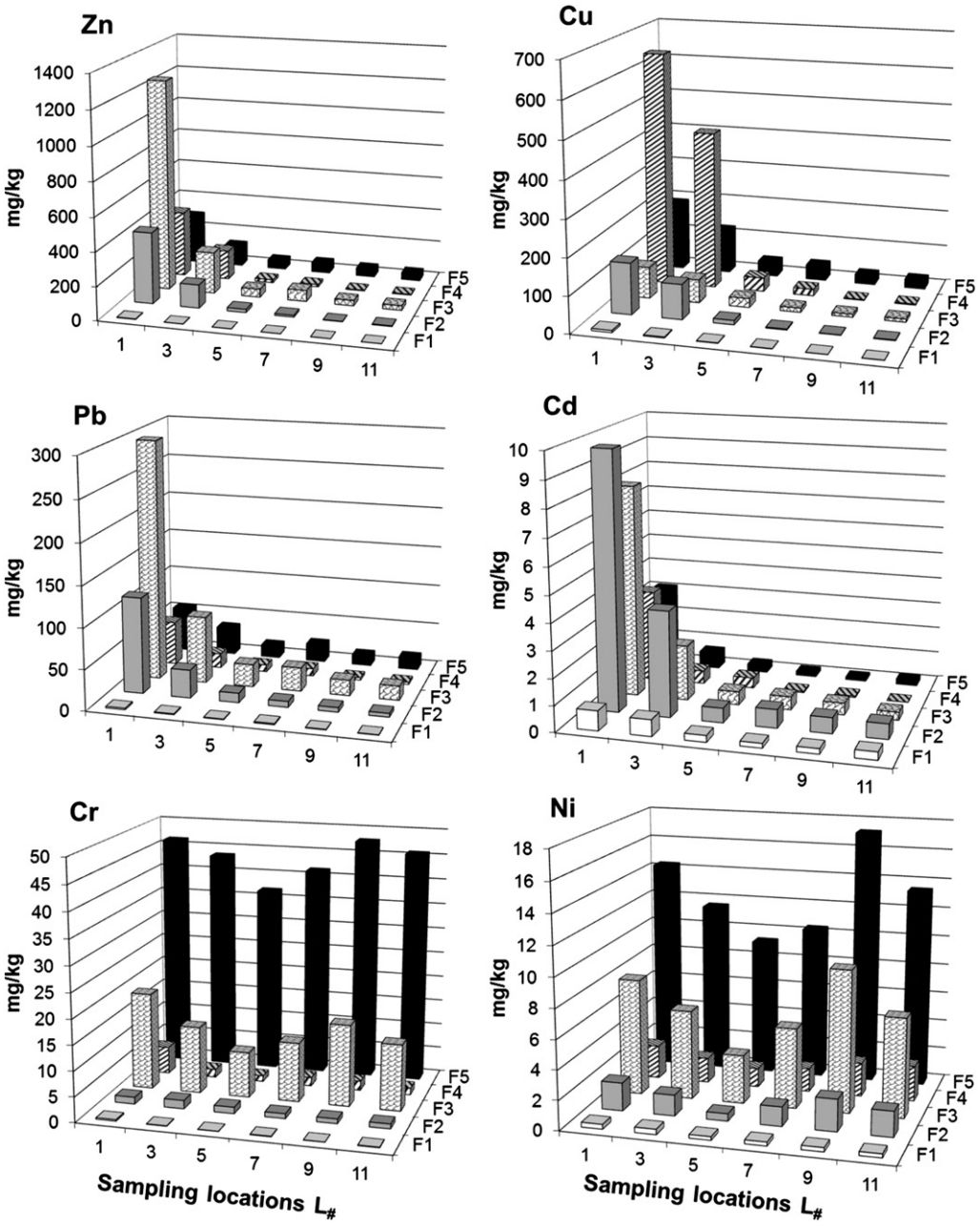

Fig. 2. Results from the sequential extractions of the soil samples collected along transect with operational fractions F1–F5 as compiled in Table 1.

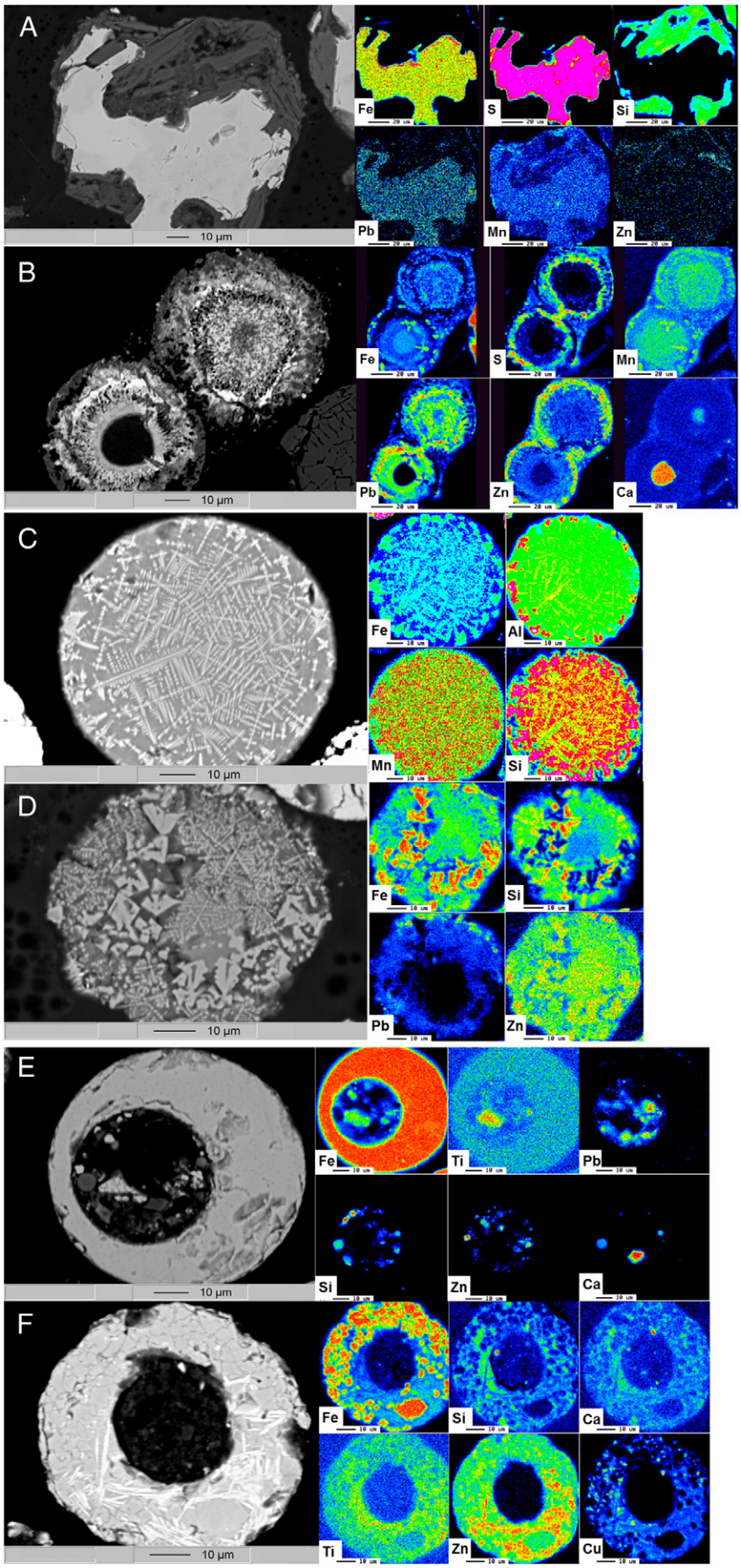
A
Fe
S
Si
Pb
Mn
Zn
10 μm
B
Fe
S
Mn
Pb
Zn
Ca
10 μm
C
Fe
Al
Mn
Si
10 μm
D
Fe
Si
Pb
Zn
10 μm
E
Fe
Ti
Pb
Si
Zn
Ca
10 μm
F
Fe
Si
Ca
Ti
Zn
Cu
10 μm

at 10–20 cm is higher, Table 5). However, no such difference was found in the Cd content at the two sampling depths, indicating that this toxic metal has a higher availability. The concentrations found of Cr (62 ± 18 mg kg^{-1}) and Ni (29 ± 7 mg kg^{-1}) showed no significant spatial trend and may represent the geogenic background values. The results of the sequential extraction of Cu, Pb, Zn, and Cd along transect are depicted in Fig. 2. In general, the quantities extracted depend again on the distance from the AMSC emission source. The amount of Cd in the first two exchangeable fractions was higher at the locations nearest to the pollution source, and decreased exponentially with increasing distance. Although relatively high amounts of Zn, Pb and Cu were also found in the exchangeable fractions at location L_1, the highest amounts were found in the acid-reducible fraction (Zn, Pb) and oxidizable fraction (Cu) (Fig. 2). This suggests that metal due to anthropogenic impact is retained in different soil host phases. There was almost no variation in the amount of Cu, Pb, Zn and Cd in fractions obtained from samples more than 12 km from the pollution source. The majority of the Ni and Cr was found in the acid-reducible and residual fractions. The amounts did not vary with distance along transect (Fig. 2), as was observed in measurements of total concentration. This indicates that Ni and Cr are less mobile than the other metals, and indicates that no significant Ni and Cr amounts were emitted by the Almalyk industrial complex.

Dissolved (i.e., <0.45 μm) metal concentrations sampled by the micro-suction cups (Me_{diss}) showed no systematic change within 5 days of aerobic incubation. This incubation time was intended to mimic soil watering events during the rainy season. The incubation result suggests fast equilibration between solid and aqueous metal speciation, and it was therefore appropriate to average the values of the 10 micro-suction cups of the duplicate soil incubations per plot. However, there were significant differences between the thus averaged values at the different locations for the metals which fell sharply with distance along transect (Table 5). The dissolved concentrations of Ni and Cr showed no systematic spatial or temporal variation, with a mean ± SD of all measurements ($n = 60$) of 15.2 ± 6.9 μg L^{-1} and 1.51 ± 0.55 μg L^{-1}, respectively. Distribution coefficients K_d calculated as the ratio between solid and dissolved metal concentrations for Cd and Zn were in the order of less than 1000 L kg^{-1}, but one order of magnitude higher for both Cr and Ni.

3.3. Particle mineralogy of the heavy mineral fraction

Gravity separation revealed that the heavy mineral fraction is about 1% near the AMSC at first two sampling plots (L_1 and L_2). It decreased with distance down to 0.25% at locations L_{10} and L_{11}, with a distance of 18–20 km from the emission sources, in parallel to the total metal concentrations. Several primary ore minerals such as galena (PbS), chalcopyrite ($CuFeS_2$), and sphalerite (ZnS) were identified by XRD in this fraction. At location L_1 near the AMSC pollution source, typical secondary weathered phases of primary sulfide ore minerals were also identified: cerussite ($PbCO_3$), hydrocerussite ($Pb(CO_3)_2OH$), anglesite ($PbSO_4$), leadhillite ($Pb_4(CO_3)_2(OH)_2SO_4$), pyromorphite ($Pb_5(PO_4)_3Cl$), malachite ($CuCO_3$), and smithsonite ($ZnCO_3$).

The microprobe BE images of the heavy mineral fraction revealed many grains and spherical particles with brightly contrasting elements, which indicates a metal-rich composition. Fine grains of sulfide ore minerals (Fig. 3a) embedded in silicate gangue material, some of them also with secondary sulfate rims due to weathering (Fig. 3b), can be related to contamination by mining activities. The absence of an oxygen peak indicates that Cu, Zn, and Pb are mainly associated either with primary sulfide or with secondary sulfate phases (oxygen not shown in the element maps). Spherical particles dominate the metal-bearing heavy mineral fraction in samples collected near the metal smelters (Fig. 3c–f). The morphology and internal microstructure of the spherical particles indicate that they were formed in a pre-existing molten phase, and probably emitted in an inefficient flue gas cleaning process. The metal-bearing microstructures within the spherical particles indicated by bright contrast in the BE images can be categorized into (i) ferriferous dendritic and euhedral or skeletal phases in a Zn- and Pb-bearing vitreous silicate matrix (Fig. 3c,d), (ii) thick homogeneous ferriferous rims with heterogeneous cores of small lumpy metal sulfide or silicate particles (Fig. 3c), and (iii) hollow spheres of metal-rich silicate matrix (Fig. 3f). The element maps indicate that Fe was abundant in most metal-bearing particles. Iron can interact with the surrounding melted calcic silico-aluminous phase to form the highly ferriferous silicate phases. Other elemental associations were also identified: Fe/S/Pb/Mn, S/Pb/Zn/Mn/Fe, or pure Cu and Zn only. The gray vitreous matrix corresponds to a phase structure mainly composed of lighter elements: Si, Al, Ti, Si and Ca, with only traces of Fe and Mn, but sometimes enriched in Zn and Pb. Dendritic phases known as harrisitics embedded in vitreous matrices are typical for high temperature smelting and combustion processes, and indicative of high melting spinel phase crystallization during quenching of the fly ashes in the flue gas purification units (Speiser et al., 2001). The harrisitic spinel phases are generally considered to be the most weathering-resistant metal host phases (Ettler et al., 2009). On the other hand, Pb- and Zn-bearing glassy silicate spheres are among the least weathering-resistant metal host phases and are prone to relatively fast weathering in soil. Occasionally, the fly ash particles contained angular grains of tiny primary ore minerals, many of these covered with secondary ore minerals such as Fe hydroxides and carbonates. Weathering appears to be accelerated in such ash that has been produced in partial reactions.

3.4. Microbiology

Fig. 4 summarizes the results obtained for the functioning parameters of the microbial soil ecosystem on the transect. Although there is a considerable variation in the results observed at each plot, it is still possible to observe spatial trends along transect. Soil microbial biomass carbon (C_{mic}) increased first slightly with distance from the AMSC pollution source, and reached a steep maximum of 335 μg g^{-1} in samples taken from the upper (0–10 cm), and 275 μg g^{-1} in lower (10–20 cm) soil layers, respectively, at plot L_6 10 km from the pollution sources. N_{mic} values showed no trend and were around 1 ± 0.5 μg g^{-1}, except of a high value of 4.35 μg g^{-1} at location L_6, and also at two other locations further away from the pollution source (L_{10} and L_{11}, Fig. 4). The value of the dimensionless microbial coefficient C_{mic}/C_{org} varied widely between the sampling locations, and the difference between the values obtained was shown to be statistically significant ($p < 0.003$) with a trend to increase with distance from the AMSC pollution source. High coefficients (of around 2.75) were observed at least 10 km from the pollution source, while the lowest coefficient values (between 0.77 and 1.85) were observed in both soil layers at location L_1 (Fig. 4). As a result of significant spatial trends in C_{mic}, the metabolic quotient qCO_2 decreased from a maximum value of 3.3 down to 0.61 mg CO_2–C (g C_{mic} h)$^{-1}$ along transect (Fig. 4). The lowest qCO_2 values were found at locations L_6 and L_9.

Significant negative correlations were found between the total or dissolved concentration of Zn, Cu, Pb, Cd and the microbial coefficient C_{mic}/C_{org} ($r = 0.62^{*} - 0.80^{**}$). Significant positive correlations were

Fig. 3. Microstructure (BE images) and element maps of metal-bearing heavy mineral particles. Samples from most polluted transect locations L_1 and L_3, with (A) fine grains of sulfide ore minerals in a silicate matrix, or (B) sulfides covered with rims of secondary minerals due to weathering, (C,D) spherical particles showing metalliferous dendrites in a silicate matrix, and (E,F) spherical particles with typical core-and-rim structures. The black bar scales to 10 μm (BE images) and 20 μm (element maps) length, respectively. Element abundance is increasing along the color spectrum from blue to red.

found between all metal concentrations and the qCO_2 values, which represent the soil ecophysiological status. The significance of the correlations was higher for the dissolved than for the total metal concentrations (Table 6). No significant correlation was found with N_{mic} and R_B (Table 6). Although the R_B values indicated that there was a significant microbial CO_2 production at all sampling sites, it did not change much between the locations, except at the plots L_1, L_5, and L_9 with a maximum three-fold lower value of around 65–70 μg CO_2–C (g soil h)$^{-1}$ (Fig. 4). No significant correlation was found between any biological parameter and the amount of metal in the exchangeable F1 or any other fraction of the sequential extractions (Table 6).

There was a relatively small population of soil free-living nematodes at the first five plots (L_1–L_5) near the pollution source, compared to the more distant locations. At the level of locations L_1–L_5, in the upper soil layer there were 32, 30, 36, 46, and 39 individuals per 100 g dry soil, and in the lower soil layer there were 29, 27, 33, 46, and 39 individuals per 100 g dry soil, respectively. The highest numbers of nematodes were observed at locations further away from the AMSC pollution source, peaking at around 80 individuals (Fig. 4). Negative correlations were found between the total nematode abundance (T_{Nem}) and both the total and dissolved metal concentrations ($r = 0.70^* - 0.89^{**}$, Table 6). Similar correlations were observed between the different nematode trophic groups and the metal concentrations. The proportion of nematodes in each trophic group varied at each sampling location, appearing to be dependent on the distance from the pollution source. The proportion of bacteriovores (*BF*) and plant-parasites (*PP*) in the lower soil layer, and omnivore-predators (*OP*) in both soil layers, increased with distance from the pollution source. However, the proportion of *BF*, *PP* and fungivores (*FF*) in the upper soil layer increased at the first three locations, and then decreased with distance from the pollution source. The proportion of *BF*, *FF*, *PP* and *OP* trophic groups to the total composition of the nematode population was 4%, 53%, 42% and 1% in the upper, and 17%, 5%, 72% and 6% in the lower soil layers near the pollution source. The proportion of the observed trophic groups at the furthest location from the pollution source was 23%, 6%, 9% and 62% in the upper, and 32%, 3%, 40%, and 26% in the lower soil layers. The proportions of the *BF* and *OP* less abundant at the contaminated sites, but not of the more abundant *FF* and *PP* species, were found to correlate with both total and dissolved concentrations of most metals in the soil along transect ($r = 0.41^* - 0.87^{**}$, Table 6).

4. Discussion

Soils in the vicinity of smelters, and other industrial plants that emit large amounts of metal-rich particles, remain contaminated with metals for a long time, unless remediation measures are taken. In our case, the

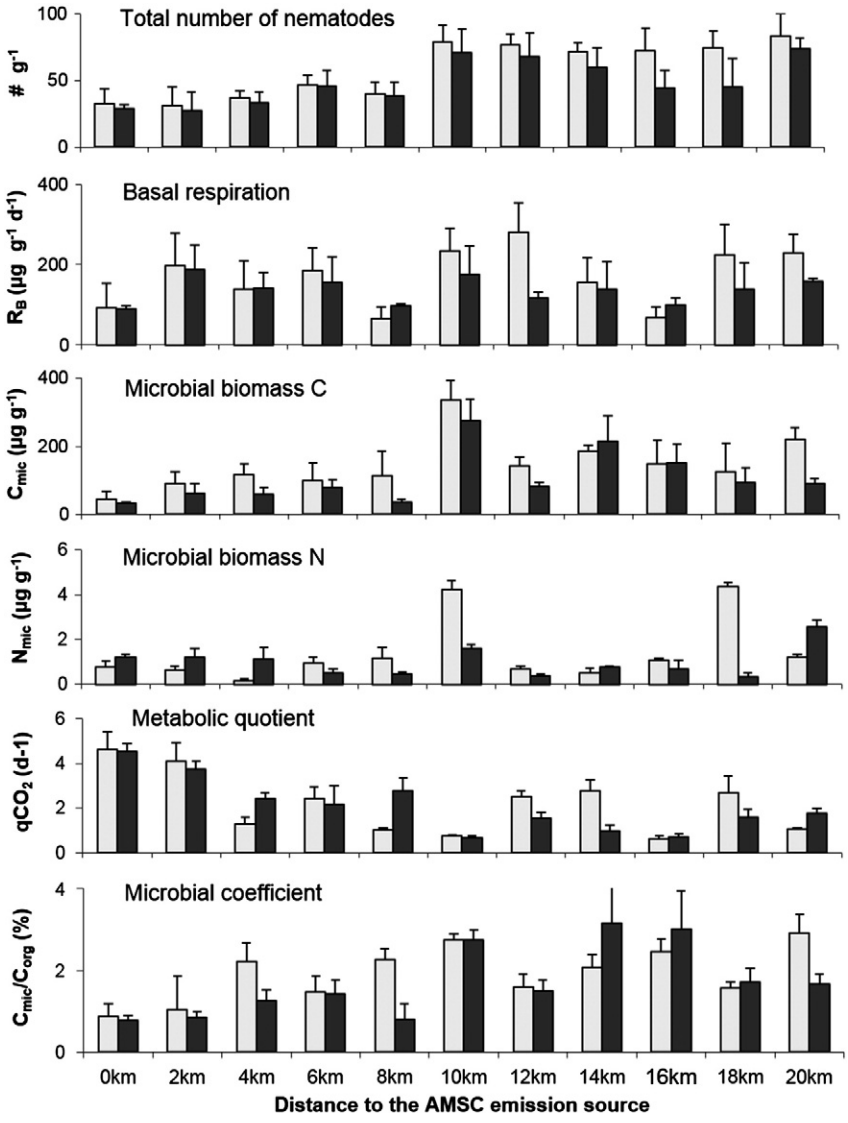

Fig. 4. Microbial ecosystem functioning parameters along transect at two soil depths (white bars 0–10 cm, black bars 10–20 cm depth).

metals (Zn, Pb, Cu, and Cd) enriched in soils were deposited in form of tiny sulfide ore mineral grains because of contamination by mining activities (Fig. 3a,b). The sulfide fines are readily oxidizable and prone to weathering, occasionally already covered with weathering rims of secondary minerals (sulfates or carbonates). The other major form of spherical metalliferous particles was found in smelter-impacted areas, which indicates that they originate from fast homogeneous condensation of pre-existing molten metal-bearing phases or even heterogeneous condensation from flue gas (Fig. 3c–f). In oxidizing melts, the metals show a lithophile behavior that favors their combination with less fusible oxides (Cr, Ni) or more fusible silicates (Zn, Pb, Cu). Occurrence of the latter thermodynamically unstable amorphous phases is critical, because they also easily weather and release their metal inventory slowly but steadily even in alkaline soils (Zevenbergen et al., 1999).

Near the AMSC industrial site, up to 30 times higher total, and up to 100 times higher dissolved concentrations of metals were recorded than in more distant locations. The presence of the metals in metastable ash particles exposed to weathering in the soils may lead to long-term mobilization. The critical labile load of anthropogenic metals may be evidenced and quantified from the changes in their binding forms (Vanek et al., 2008; Ettler et al., 2012). In fact, a higher proportion of the metals appeared in the first four fractions of our sequential extractions near the pollution source, except for Ni and Cr. This suggests that neoformation of anthropogenic metal binding forms has taken place for Cd, Cu, and Pb. The release and bioavailability of the latter metals are obviously related to the weathering sensitivity of their metastable host phases, observed by electron microscopy, and the solubility of the secondary metal-bearing precipitates. To evaluate the nature of these precipitates, we performed additional thermodynamic equilibrium calculations using the software Visual MINTEQ Ver. 3.0 (www2.lwr.kth.se/English/OurSoftware/vminteq/). The saturation indices (*SI*) calculated for the dissolved metal concentrations in the equilibrated soil incubations for pH 8 and ambient CO_2 partial pressure indicated that the soil solutions from location L_1 are nearly at equilibrium ($-0.5 < SI < 0.5$) with respect to $ZnCO_3$, $CdCO_3$, and $CuCO_3$. This result is corroborated by the increase of the concentrations of these metals in step F2 of the sequential extractions (Fig. 2) and also by the secondary carbonate phases of these metals identified by XRD. Carbonates have been already observed as important secondary alteration products in slags and ashes from smelters at other locations (Vanek et al., 2008; Ettler et al., 2009, 2012). This result is also in agreement with previously published experimental data in which the neoformation of Pb, Zn and Cd carbonates on fly ash particles was described (Birkefeld et al., 2007; Cecchi et al., 2008; Nowack et al., 2010). In these studies, the carbonates occurred with circumneutral to slightly alkaline soils within a few months of incubation. Overall, the data from our different analytical approaches add to a well integrated and conclusive idea about the mechanisms of soil contamination downwind of the Almalyk industrial complex.

For the impact of the contamination on soil health, we found that the microbial biomass C_{mic}, and the microbial coefficient C_{mic}/C_{org}, increased gradually along transect in response to the decrease in metal concentration and availability observed in both soil layers. The ecophysiological quotient qCO_2 used to evaluate the environmental impact on the soil microbial community showed a gradual decrease toward the end of the transect, and hence a positive correlation with the metal contamination. The relationship with the biological parameters was more significant for the dissolved than for the total metal concentrations, but not significant for the extractable metal portions (Table 6). The microbial parameters reported here are within the range of values reported by Hofman et al. (2003) who studied microbial biomass and respiration to determine the relationships between soil properties and contamination. In agreement with those results, we found both the microbial coefficient C_{mic}/C_{org} and ecophysiological quotient qCO_2 quite useful gaining more complete understanding of the interaction between soil chemical and soil microbial composition. The microbial coefficient can be interpreted to being indicative of substrate bioavailability. Since the microbial coefficient exhibited a most significant increase in an inverse manner to the significant decrease in the ecophysiological status, both parameters seem to complement the sensitivity of the microbial community to soil contamination. We conclude that both parameters are the most useful bioindicators of soil pollution, together with the water-soluble metal concentration.

5. Conclusions

The AMSC is located in a semiarid Central Asian region, which encounters seasonal variations in precipitation. We have shown that this climate can retard but not hinder the weathering of the metastable primary sulfidic and silicate ash phases and formation of more soluble secondary carbonate phases. The high bioavailability of Cd, Cu and Zn

Table 6
Correlation coefficients between soil biological activity and metal concentrations along the 20 km transect downwind of the AMSC emission source.

	T_{Nem}	R_B	C_{mic}/C_{org}	qCO_2	*nBF*	*nFF*	*nPP*	*nOP*
Total organic carbon (C_{org})	**0.63***	**0.81****	0.28	−0.14	−0.14	**0.60***	0.04	0.28
Total soluble nitrogen (*TSN*)	0.25	0.51	−0.29	0.27	0.09	−0.08	0.06	0.05
C_{mic}	**0.78****	0.41	**0.84****	**−0.61***	0.25	0.56	−0.21	0.38
N_{mic}	0.50	0.21	0.16	−0.21	0.37	0.29	−0.19	**0.89****
Ca^{2+}	0.10	0.33	−0.24	0.26	0.19	−0.32	−0.41	−0.21
Na^{+}	0.14	−0.46	0.14	−0.23	0.47	**−0.65***	−0.41	0.54
K^{+}	0.55	**0.74****	−0.01	0.08	0.04	0.30	−0.08	0.59
Zn_{total}	**−0.81****	−0.16	**−0.70****	**0.67****	**−0.79****	0.31	0.21	**−0.84****
Zn_{ex}	−0.28	0.12	−0.13	0.17	−0.29	0.15	0.31	−0.32
Zn_{diss}	**−0.88****	−0.23	**−0.73****	**0.76****	**−0.75****	−0.43	0.16	−0.53
Cu_{total}	**−0.89****	−0.12	**−0.63****	**0.62****	**−0.86****	−0.22	0.12	**−0.76****
Cu_{ex}	−0.29	0.20	−0.17	0.39	−0.39	0.14	0.40	−0.30
Cu_{diss}	**−0.86****	−0.10	**−0.75****	**0.80****	**−0.87****	−0.22	0.14	−0.49
Pb_{total}	**−0.70****	−0.22	**−0.66****	**0.63****	**−0.83****	−0.31	0.32	**−0.83****
Pb_{ex}	−0.21	−0.39	−0.17	0.39	−0.48	−0.14	**0.57***	**−0.51***
Pb_{diss}	**−0.71****	−0.19	**−0.80****	**0.78****	−0.41	−0.43	−0.07	0.08
Cd_{total}	**−0.54***	−0.13	**−0.59***	0.47	−0.29	−0.44	0.15	**−0.82****
Cd_{ex}	−0.24	0.27	−0.15	0.20	−0.14	−0.23	**0.57****	−0.12
Cd_{diss}	**−0.73****	−0.09	**−0.60***	**0.60***	**−0.85****	−0.19	0.23	**−0.65***
Cr_{total}	0.25	0.29	−0.18	0.30	0.45	−0.29	−0.38	0.15
Ni_{total}	0.41	0.18	0.03	0.04	**0.76****	−0.29	−0.53	0.21

T_{Nem} — total nematode abundance, R_B — Basal respiration, *nBF* — number of bacteriovores, *nFF* — number of fungivores, *nPP* — number of plant-parasites, *nOP* — number of omnivore-predators nematode trophic groups. Me_{total} — total metal concentration (XRF) in soil (n = 44); Me_{ex} — NaOAc-exchangeable (F1) metal concentration (n = 22); Me_{diss} — dissolved metal concentration in soil porewater (n = 12); linear correlation coefficients *r* printed in bold are significant at $p < 0.05^{*}$ and $p < 0.01^{**}$, respectively.

evidenced by the geochemical experiments with soil wetting may lead to their vertical migration in the soil profiles. We observed enrichments of these metals (in particular of the most mobile Cd) in the deeper soil layers similarly as has been documented at numerous other smelter-affected sites (e.g., Nowack et al., 2010; Chrastny et al., 2012). Furthermore, the results presented here reveal remarkable spatial differences in metal geochemistry, not only in the metal concentrations, but also in the metal partitioning in the sequential extractions. We observed substantial enrichments of both Zn and Cd in the acid-reducible fraction and of Cu in the oxidizable fraction near the pollution source L_1 (Fig. 2). These results indicate initiation of repartitioning processes for the metals from the weathered ash particles via the solution to natural soil minerals such as Fe oxyhydroxides and humic matter. The dissolved Pb concentrations already at location L_1, and metal concentrations at all other locations, are all undersaturated with respect to their carbonate minerals, and therefore controlled by mechanisms other than carbonate solubility. Pb is known to be immobilized by strong adsorption to ambient natural soil minerals such as Fe hydroxides (Kersten et al., 1997). This hypothesis is corroborated by the sequential extraction results, which show the highest enrichments for Pb (but high enrichments also for other metals) in the acid-reducible fraction at the polluted location L_1 (Fig. 2).

The results reveal also a remarkable spatial dependence in the microbiological soil health properties along transect downwind from the AMSC emission source. We have identified an inverse relationship between the pollutant concentration in the soil and microbial ecosystem functioning parameters, as supported by similar studies at polluted soil sites (Kandeler et al., 1996, 1999). This study corroborates the effectiveness of nematode density, biomass, activity, and trophic group distribution as bioindicators of soil ecosystem health also in industrial semi-arid areas. It demonstrates the potential of this technique as an integral tool for triad approaches of environmental ecotoxicity risk assessment to develop and evaluate best management practices of contaminated soils of Central Asia. Based on the results of this study and of previous investigations in adjacent regions (Shukurov et al., 2006, 2009; Pen-Mouratov et al., 2010), we recommend rigorous environmental monitoring of all industrial regions as part of the national environmental monitoring program using those parameters. An understanding of how ecosystem functioning parameters vary with degree of pollution in those regions is, however, not only useful to quantify the anthropogenic impact on soil health, but also to assess the efficacy of any future remediation activities.

As an additional feature of this study, it was shown that the soil free-living nematode density and taxa is also a sensitive indicator of unpolluted soil, and therefore could become useful for evaluation of any future soil remediation efforts. We have analyzed the food consumption characteristics of nematode populations in the study area to understand how the populations respond to metal pollution. We showed that plant parasites, followed by fungi-feeding nematodes, were the most dominant trophic groups close to the AMSC emission source. Moving away from the pollution source along transect, this dominance was replaced by bacteria-feeding and omnivore-predator nematodes. Our data are in agreement with older studies, where an addition of Cu, Ni and Zn of up to 1600 mg kg^{-1} significantly affected many parameters of the nematode community structure (Parmelee et al., 1993; Korthals et al., 1996b). Clearly, many environmental factors have the potential to affect nematode community, which consequently results in high space and time variability. This variance is a known major handicap in field ecotoxicological studies because pollutant–nematode relationships may become obscured (Sochova et al., 2006), but not necessarily as shown in the present case.

Acknowledgments

These investigations were supported by an INTAS YS Fellowship (Ref. No. 04-83-2623) and a George Forster Research Fellowship by the Alexander-von-Humboldt Foundation (Ref. No. 1148710STP) to the first author. The authors are grateful for the assistance of Nora Groschopf in SEM/EDX analysis, and of Carolin Berg in ICP analysis. Ginetta Barnes provided advices and technical assistance on the microbiological analyses.

Appendix A. Supplementary data

Supplementary data associated with this article can be found in the online version, at http://dx.doi.org/10.1016/j.scitotenv.2014.01.031. These data include Google maps of the most important areas described in this article.

References

Anderson TH, Domsch KH. Application of eco-physiological quotients (qCO_2 and qD) on microbial biomass from soils of different cropping histories. Soil Biol Biochem 1990;22:251–5.
Bakonyi G, Nagy P, Kadar I. Long-term effects of heavy metals and microelements on nematode assemblage. Toxicol Lett 2003;140:391–401.
Bardgett RD, Speir TW, Ross DJ, Yeates GW, Kettles HA. Impact of pasture contamination by copper, chromium, and arsenic timber preservative on soil microbial properties and nematodes. Biol Fertil Soils 1994;18:71–9.
Birkefeld A, Schulin R, Nowack B. In situ transformations of fine lead oxide particles in different soils. Environ Pollut 2007;145:554–61.
Bongers T, Bongers M. Functional diversity of nematodes. Appl Soil Ecol 1998;10:239–51.
Brookes PC. Use of microbial parameters in monitoring soil pollution by heavy metals. Biol Fertil Soils 1995;19:269–79.
Cairns EJ. Methods in nematology. In: Sasser JN, Jenkins WR, editors. Nematology — fundamentals and recent advances with emphasis on plant parasitic and soil forms. Chapel Hill: University of North Carolina Press; 1960. p. 33–84.
Cappuyns V, Swennen R, Niclaes M. Application of the BCR sequential extraction scheme to dredged pond sediments contaminated by Pb–Zn mining: a combined geochemical and mineralogical approach. J Geochem Explor 2007;93:78–90.
Caussy D, Gochfeld M, Gurzau E, Neagu C, Ruedel H. Lessons from case studies of metals: investigating exposure, bioavailability, and risk. Ecotoxicol Environ Saf 2003;56:45–51.
Cecchi M, Dumat C, Alric A, Felix-Faure B, Pradere P, Guiresse M. Multi-metal contamination of a calcic cambisol by fallout from a lead-recycling plant. Geoderma 2008;144:287–98.
Chrastny V, Vanek A, Komarek M, Farkas J, Drabek O, Vokurkova P, et al. Incubation of air pollution control residues from secondary Pb smelter in deciduous and coniferous organic soil horizons: leachability of lead, cadmium and zinc. J Hazard Mater 2012;209–210:40–7.
Cohen D, Shen X, Dunlop A, Rutherford N. A comparison of selective extraction soil geochemistry and biogeochemistry in the Cobar area, New South Wales. J Geochem Explor 1998;61:173–89.
Dold B. Speciation of the most soluble phases in a sequential extraction procedure adapted for geochemical studies of copper sulfide mine waste. J Geochem Explor 2003;80:55–68.
EPA. Understanding variation in partition coefficient, Kd, values. Volume II: review of geochemistry and available Kd values for Cd, Cs, Cr, Pb, Pu, Rn, Sr, Th, tritium (^3H), and U; August 1999 [Washington. http://www.epa.gov/radiation/docs/kdreport/vol2/402-r-99-004b.pdf].
Ettler V, Johan Z, Kribek B, Sebek O, Mihaljevic M. Mineralogy and environmental stability of slags from the Tsumeb smelter, Namibia. Appl Geochem 2009;24:1–15.
Ettler V, Mihaljevic M, Sebek O, Grygar TM, Klementova M. Experimental in situ transformation of Pb smelter fly ash in acidic soils. Environ Sci Technol 2012;46:10539–48.
Fanfani L, Zuddas P, Chessa A. Heavy metals speciation analysis as a tool for studying mine tailings weathering. J Geochem Explor 1997;58:241–8.
FAO. Fertilizer use by crop in Uzbekistan. Rome: FAO; 2003 [41 pp. ftp://ftp.fao.org/agl/agll/docs/fertuseuzbekistan.pdf accessed June 2013].
Favas PJC, Pratas J, Gomes MEP, Cala V. Selective chemical extraction of heavy metals in tailings and soils contaminated by mining activity: environmental implications. J Geochem Explor 2011;111:160–71.
Hattori H. Influence of heavy metals on soil microbial activities. Soil Sci Plant Nutr 1992;38:93–100.
Heinemayer O, Insam H, Kaiser EA, Walenzik G. Soil microbial biomass and respiration measurements: an automated technique based on infrared gas analysis. Plant Soil 1989;116:191–5.
Hofman J, Bezchlebova J, Dusek L, Dolezal L, Holoubek I, Andel P, et al. Novel approach to monitoring of the soil biological quality. Environ Int 2003;28:771–8.
Houba VJG, Novozamsky I, Vittenbogaard J, Van Der Lee JJ. Automatic determination of total soluble nitrogen in soil extracts. Landwirtsch Forsch 1987;40:295–302.
Ingham ER, Trofymow JA, Ames RN, Hunt HW, Morley CR, Moore JC, et al. Trophic interactions and nitrogen cycling in a semiarid grassland soil. 1. Seasonal dynamics of the natural populations, their interactions and effects on nitrogen cycling. J Appl Ecol 1986a;23:597–614.
Ingham ER, Trofymow JA, Ames RN, Hunt HW, Morley CR, Moore JC, et al. Trophic interactions and nitrogen cycling in a semiarid grassland soil. 2. System responses to removal of different groups of soil microbes or fauna. J Appl Ecol 1986b;23:615–30.

Jänsch S, Römbke J, Didden W. The use of enchytraeids in ecological soil classification and assessment concepts. Ecotoxicol Environ Saf 2005;62:266–77.
Joergensen RG, Mueller T. The fumigation — extraction method to estimate soil microbial biomass: calibration of the k_{EN} value. Soil Biol Biochem 1996;28:33–7.
Kaiser EA, Mueller T, Joergensen RG, Insam H, Heinemeyer O. Evaluation of methods to estimate the soil microbial biomass and the relationship with soil texture and organic matter. Soil Biol Biochem 1992;24:675–83.
Kandeler E, Kampichler C, Horak O. Influence of heavy metals on the functional diversity of soil microbial communities. Biol Fertil Soils 1996;23:299–306.
Kandeler E, Tscherko D, Spiegel H. Long-term monitoring of microbial biomass, N mineralisation and enzyme activities of a Chernozem under different tillage management. Biol Fertil Soils 1999;28:343–51.
Kapusta P, Szarek-Lukaszewska G, Stefanowicz AM. Direct and indirect effects of metal contamination on soil biota in a Zn–Pb post-mining and smelting area (S Poland). Environ Pollut 2011;159:1516–22.
Kersten M, Förstner U. Speciation of trace metals in sediments and combustion waste. In: Ure AM, Davidson CM, editors. Chemical speciation in the environment. London: Chapman & Hall; 1995. p. 234–75.
Kersten M, Moor MC, Johnson CA. Speciation of trace metals in leachate from a MSWI bottom ash landfill. Appl Geochem 1997;12:675–83.
Klumpp A, Hintemann T, Lima JS, Kandeler E. Bioindication of air pollution effects near a copper smelter in Brazil using mango trees and soil microbiological properties. Environ Pollut 2003;126:313–21.
Kodirov O, Shukurov N. Heavy metal distribution in soils near the Almalyk mining and smelting Industrial area, Uzbekistan. Acta Geol Sin-Engl 2009;83:985–90.
Korthals GW, Van de Ende A, Van Megen H, Lexmond TM, Kammenga JE, Bongers T. Short-term effects of cadmium, copper, nickel and zinc on soil nematodes from different feeding and life-history strategy groups. Appl Soil Ecol 1996a;4:107–17.
Korthals GW, Alexiev AD, Lexmond TM, Kammenga JE, Bongers T. Long-term effects of copper and pH on the nematode community in an agroecosystem. Environ Toxicol Chem 1996b;15:979–85.
Levine RM, Wallace GJ. The mineral industry of Uzbekistan. U.S. Geological Survey, 2007 Minerals Yearbook; 2010 [http://minerals.usgs.gov/minerals/pubs/country/2007/myb3-2007-uz.pdf accessed June 2013].
Li X, Thornton I. Chemical partitioning of trace and major elements in soils contaminated by mining and smelting activities. Appl Geochem 2001;16:1693–706.
Liang W, Pinhasi-Adiv Y, Shultz H, Steinberger Y. Nematode population dynamics under the canopy of desert halophytes. Arid Soil Res Rehabil 2000;1:183–92.
Martín F, Diez M, García I, Simón M, Dorronsoro C, Iriarte Á, et al. Weathering of primary minerals and mobility of major elements in soils affected by an accidental spill of pyrite tailing. Sci Total Environ 2007;378:49–52.
Nahmani J, Rossi J. Soil macroinvertebrates as indicators of pollution by heavy metals. C R Biol 2003;326:295–303.
Neher DA. Role of nematodes in soil health and their use as indicators. J Nematol 2001;33:161–8.
Nowack B, Schulin R, Luster J. Metal fractionation in a contaminated soil after reforestation: temporal changes versus spatial variability. Environ Pollut 2010;158:3272–8.
Parmelee RW, Wentsel RS, Phillips CT, Simini M, Checkai RT. Soil microcosm for testing the effects of chemical-pollutants on soil fauna communities and trophic structure. EnvironToxicol Chem 1993;12:1477–86.
Peijnenburg WJ, Zablotskaja M, Vijver MG. Monitoring metals in terrestrial environments within a bioavailability framework and a focus on soil extraction. Ecotoxicol Environ Saf 2007;67:163–79.
Pen-Mouratov S, Shukurov N, Steinberger Y. Soil free-living nematodes as indicators of both industrial pollution and livestock activity in Central Asia. Ecol Indic 2010;10:955–67.
Pueyo M, Mateu J, Rigol A, Vidal M, López-Sánchez JF, Rauret G. Use of the modified BCR three-step sequential extraction procedure for the study of trace element dynamics in contaminated soils. Environ Pollut 2008;152:330–41.
Rais D, Nowack B, Schulin R, Luster J. Sorption of trace metals by standard and micro suction cups in the absence and presence of dissolved organic carbon. J Environ Qual 2006;35:50–60.
Rowell DL. Soil science: methods and applications. London: Longmans Group UK Ltd.; 1994.
Santorufo L, Van Gestel CAM, Rocco A, Maisto G. Soil invertebrates as bioindicators of urban soil quality. Environ Pollut 2012;161:57–63.
Shao Y, Zhang W, Shen J, Zhou L, Xia H, Shu W, et al. Nematodes as indicators of soil recovery in tailings of a lead/zinc mine. Soil Biol Biochem 2008;40:2040–6.
Shukurov N, Pen-Mouratov S, Steinberger Y. The impact of the Almalyk industrial complex on soil chemical and biological properties. Environ Pollut 2005;136:331–40.
Shukurov N, Pen-Mouratov S, Steinberger Y. The influence of soil pollution on soil microbial biomass and nematode community structure in Navoiy Industrial Park, Uzbekistan. Environ Int 2006;32:1–11.
Shukurov N, Pen-Mouratov S, Steinberger Y, Kersten M. Soil biogeochemical properties of Angren industrial area, Uzbekistan. J Soils Sediment 2009;9:206–15.
Smolders E, Oorts K, Van Sprang P, Schoeters I, Janssen CR, McGrath SP, et al. Toxicity of trace metals in soil as affected by soil type and aging after contamination: using calibrated bioavailability models to set ecological soil standards. Environ Toxicol Chem 2009;28:1633–42.
Sochova I, Hofman J, Holoubek I. Using nematodes in soil ecotoxicology. Environ Int 2006;32:374–83.
Sparling GP, West AW. A comparison of gas chromatography and differential respirometer methods to measure soil respiration and to estimate the soil microbial biomass. Pedobiologia 1990;34:103–12.
Sparling GP, Zhu C. Evaluation and calibration of biochemical methods to measure microbial biomass C and N in soils from Western Australia. Soil Biol Bioch 1993;25:1793–801.
Speiser C, Baumann T, Niessner R. Characterization of municipal solid waste incineration (MSWI) bottom ash by scanning electron microscopy and quantitative energy dispersive X-ray microanalysis (SEM/EDX). Fresenius J Anal Chem 2001;370:752–9.
Steinberger Y, Loboda I. Nematode population dynamics and trophic structure in a soil profile under the canopy of the desert shrub *Zygophyllum dumosum*. Pedobiologia 1991;35:191–7.
Steinberger Y, Sarig S. Responses by soil nematode populations in the soil microbial biomass to a rain episode in the hot, dry Negev Desert. Biol Fert Soils 1993;16:188–92.
Tessier A, Campbel PGC, Bisson M. Sequential extraction procedure for the speciation of particulate trace metals. Anal Chem 1979;51:844–51.
UNECE. 1st environmental performance review Uzbekistan. Environmental performance reviews series no.14. New York and Geneva: United Nations; 2001 [182 pp. http://www.unece.org/fileadmin/DAM/env/epr/epr_studies/uzbekistan%20e.pdf [accessed June 2013].
Van Gestel CAM. Physico-chemical and biological parameters determine metal bioavailability in soils. Sci Total Environ 2008;406:385–95.
Van Herck P, Vandecasteele C. Evaluation of the use of a sequential extraction procedure for the characterization and treatment of metal containing solid waste. Waste Manag 2001;21(8):685–94.
Vanek A, Ettler V, Grygar T, Boruvka L, Sebek O, Drabek O. Combined chemical and mineralogical evidence for heavy metal binding in mining- and smelting-affected alluvial soils. Pedosphere 2008;18:464–78.
Vig K, Megharaj M, Sethunathan N, Naidu R. Bioavailability and toxicity of cadmium to microorganisms and their activities in soil: a review. Adv Environ Res 2003;8:121–35.
Weber J, Karczewska A. Biogeochemical processes and the role of heavy metals in the soil environment. Geoderma 2004;122:105–7.
Yan S, Singh AN, Fu S, Liao C, Wang S, Li Y, et al. A soil fauna index for assessing soil quality. Soil Biol Biochem 2012;47:158–65.
Yang Y, Campbell CD, Clark L, Cameron CM, Paterson E. Microbial indicators of heavy metal contamination in urban and rural soils. Chemosphere 2006;63:1942–52.
Yeates GW, Percival HJ, Parshotam A. Soil nematode responses to year-to-year variation of low levels of heavy metals. Aust J Soil Res 2003;41:613–25.
Zevenbergen C, Bradley JP, Van Reeuwijk LP, Shyam N, Hjelmar O, Comans RNJ. Clay formation and metal fixation during weathering of coal fly ash. Environ Sci Technol 1999;33:3405–9.